

A COMPARISON OF THE NEAR-INFRARED AND VISIBLE SPECTRA OF THREE BRIGHT CEPHEIDS

R. PAUL BUTLER

Department of Physics and Astronomy, San Francisco State University, San Francisco, CA 94132 and
Astronomy Department, University of California, Berkeley, CA 94720; paul@further.berkeley.edu

AND

ROGER A. BELL

Astronomy Department, University of Maryland, College Park, MD 20742; rabell@astro.umd.edu

Received 1996 September 9; accepted 1996 November 15

ABSTRACT

Recent studies have suggested that significant differences may exist between the IR and the visible radial velocity curves and line profiles for Cepheid variable stars. Such wavelength-dependent phenomena would affect the relationship between pulsational and radial velocities and the derived surface brightness (Baade-Wesselink) distances for Cepheids. In a further investigation of this problem, radial velocity curves and line profile asymmetries have been obtained from 100 absorption lines in the near-IR (8000 Å) for the bright Cepheids δ Cep (5 day period), η Aql (7 day), and X Cyg (16 day). A fiducial wavelength scale has been provided by the embedded telluric absorption lines. The relative radial velocity errors of individual stellar absorption lines have been reduced to a few hundred meters per second.

The shape and amplitude of velocity curves from lines in the near-IR are very similar to those from lines of the same atomic species and similar excitation observed in the visible region. For the two shorter period Cepheids in this study, the near-IR and visible velocity curves differ by less than 1 km s^{-1} . The longer period Cepheid X Cyg shows velocity differences of as much as 3 km s^{-1} .

The near-IR line profile asymmetries are very similar to those observed in the visible. As in the case of the visible lines, the high excitation potential (high-EP) lines in the near-IR appear to have a greater asymmetry amplitude than the low-EP lines.

Radial velocity curves and line profiles for $H\alpha$ and $H\beta$ have also been obtained. The Cepheids in this sample show a clear trend with increasing pulsation period. The $H\alpha$ and $H\beta$ line profiles of the shortest period star (δ Cep) remain relatively symmetric throughout the entire pulsation cycle, and their respective radial velocity curves remain continuous at maximum infall velocity. The $H\beta$ radial velocity curve shows only small deviations from that of the standard (Fe I) velocity curve. The $H\beta$ line of the longer period star, η Aql, remains relatively symmetric, but $H\alpha$ becomes extremely asymmetric near the phase of maximum infall. The $H\alpha$ radial velocity amplitude is 57% larger than the standard Fe I velocity curve. Both the $H\alpha$ and $H\beta$ velocity curves are very sharply peaked (almost discontinuous) at maximum infall velocity, and they lag the standard velocity curve (derived from strong 3–6 eV Fe I lines in the 5000–6300 Å region) by 0.06 in phase. Both $H\alpha$ and $H\beta$ show extreme asymmetries. For the longest period Cepheid in the sample, X Cyg, the $H\alpha$ profile splits into two components for half the pulsation cycle. The $H\alpha$ radial velocity curve is completely out of phase with the standard velocity curve, while the $H\beta$ velocity curve remains relatively well behaved, lagging the Fe I velocity curve by 0.12 in phase.

Subject headings: Cepheids — infrared: stars — line: profiles — stars: oscillations — techniques: radial velocities

1. INTRODUCTION

For most of this century, pulsating stars within the instability strip have played a critical role in setting the galactic and extragalactic distance scale. In particular, it is remarkable that the Cepheid period-luminosity (P - L) relationship continues to serve as a foundation of the extragalactic distance scale. Indeed, one of the chief justifications for building, and then repairing, the *Hubble Space Telescope* was to obtain photometric data of the Cepheids in Virgo Cluster galaxies (Freedman et al. 1994).

Detailed studies of galactic Cepheids remain vitally relevant as the primary means of establishing the absolute zero point of the Cepheid P - L relationship. The two most precise current methods of determining the distance to galactic Cepheids are the surface brightness method (Barnes-Evans or Baade-Wesselink; Wesselink 1946, 1969; Barnes et al. 1977) and main-sequence fitting to those few open clusters

and associations that have Cepheid members. Each method suffers from its own problems. Distance determinations from surface brightness techniques require phased photometric and radial velocity measurements and, thus, are afflicted by observational errors, as well as errors in the assumed color-temperature relation and the conversion from radial to pulsation velocity. Errors in the determination of the reddenings and metallicities of the 30 or so cluster and association Cepheids directly affect distance determinations at the level of a few tenths of a magnitude. Furthermore, there is the difficulty in positively determining membership for the long-period Cepheids in large associations. Unfortunately, these two methods have historically given systematically different results at the 0.1 to 0.3 mag level (Ferne 1984; Böhm-Vitense et al. 1989; Gieren & Fouque 1993), resulting in uncertainties in the derived distances at the 10%–20% level.

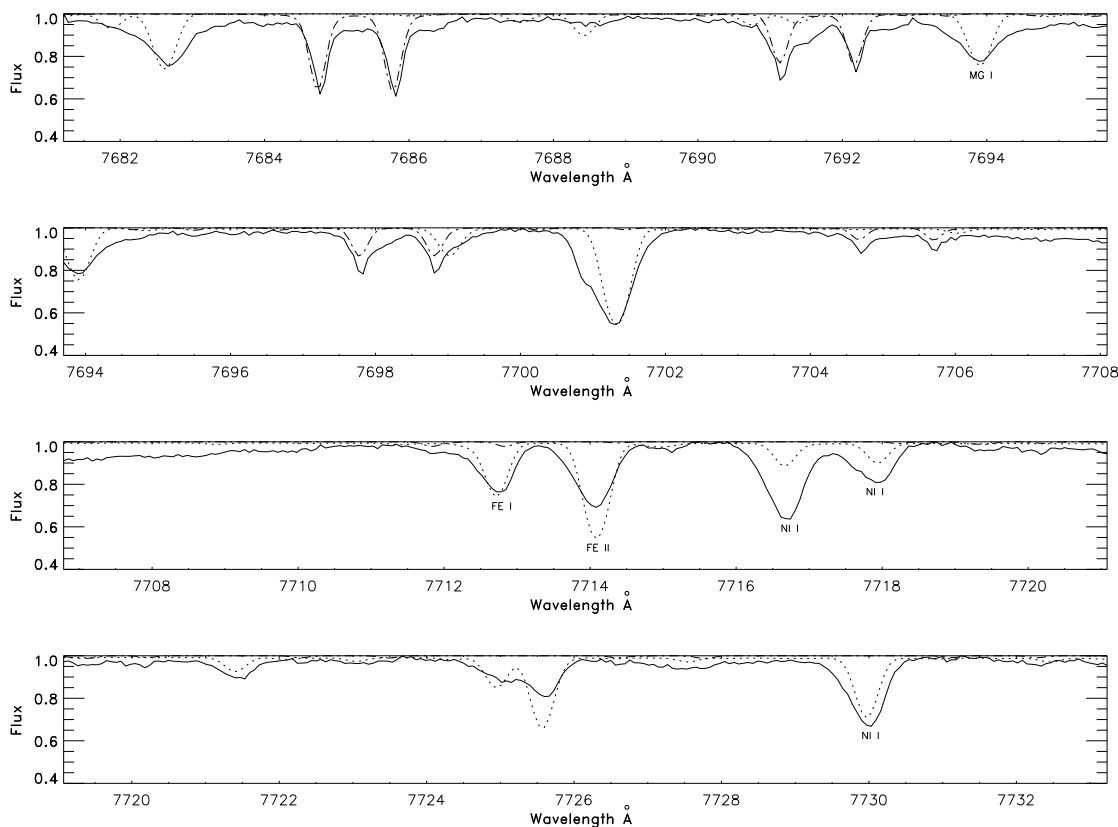


FIG. 1.—Comparison of synthetic spectra to an observed spectrum obtained with the “Hamilton” echelle spectrograph. The solid line is order 7 of η Aql taken 1990 August 28. The dot-dash line is a telluric spectrum, and the dotted line is a synthetic spectrum.

Over the last 20 yr much progress has been made on refining the Cepheid surface brightness technique, in particular on the photometric side. Barnes & Evans (1976) have shown that a much tighter color-temperature relation can be found using the $V-R$ color index instead of the classic Baade-Wesselink $B-V$ index, while recent work on Cepheids and RR Lyrae stars suggests that the $V-K$ index will further improve the temperature determination. However, precision optical interferometric systems should obviate the need for photometric data altogether within a few years (Sasselov & Karovska 1994).

These continuing photometric improvements have put the onus on the spectrographic side, especially to improve the radial velocity measurements and the conversion from radial to pulsational velocity. Over the last 5 years, a number of groups have undertaken high-resolution studies of Cepheids (Sasselov & Lester 1990; Wallerstein et al. 1992; Butler 1993; Breitfellner & Gillet 1993a, 1993b, 1993c; Albrow & Cottrell 1994). Based on variable line profile asymmetries, all of these studies have cast serious doubt on the traditional Baade-Wesselink/Barnes-Evans (hereafter BE/BW) assumption that Cepheid atmospheres are comoving. The situation is further complicated by the line asymmetries and velocity gradients introduced as a result of granulation and other phenomena in the stellar atmospheres (Dravins 1995, and references therein).

In a previous paper (Butler 1993, hereafter Paper I), Cepheid radial velocity curves were constructed from several hundred lines in the visible region. An iodine absorption cell (Marcy & Butler 1992; Butler et al. 1996b) was used to provide precise radial velocity measurements.

Radial velocity differences of several kilometers per second were seen during the phase of maximum infall velocity for various sets of lines, in agreement with the results of Sanford (1956). In a subsequent paper (Butler, Bell, & Hindsley 1996a, hereafter Paper II) model Cepheid spectra with embedded photospheric velocity gradients were constructed. It was shown that the pulsational velocity curve is reduced by about 20% by taking velocity gradients into account. The derived BE/BW distance is reduced by a similar amount.

Sasselov, Lester, & Fieldus (1989) have suggested that Cepheid radial velocity curves determined from IR (11000 Å) lines have a significantly larger amplitude than do those found from lines in the visible. Some such variation is expected, owing to the dependence of the relationship between pulsational and radial velocity on limb darkening, which is expected to vary with wavelength. In addition, any velocity gradient in the photosphere will make different contributions at different wavelengths, owing to the variation of the continuous opacity. This problem was studied in Paper II, although data covering only a small wavelength range were available. In this paper, a detailed comparison is made of radial velocity curves obtained from moderately high resolution ($\lambda/\Delta\lambda = 40000$) spectra in the visible and the near-IR for the bright Cepheids δ Cep, η Aql, and X Cyg. Precise velocity curves of near-IR lines have been constructed with the use of telluric lines, primarily due to water vapor, as reference lines (Griffin & Griffin 1973a, 1973b; Cochran et al. 1991). Section 2 of this paper will describe the observations and reduction. A comparison of 5500 Å and 8000 Å radial velocity curves will be made in § 3. Radial

velocity curves and line profiles for $H\alpha$ and $H\beta$ are given in § 4. Section 5 will report on line asymmetries, and § 6 contains the discussion.

2. OBSERVATIONS AND REDUCTION

Traditional methods of measuring stellar radial velocities, which derive wavelengths from comparison spectra, are seldom more accurate than 1 km s^{-1} . Griffin & Griffin (1973a) pointed out that instrumental errors could be minimized if a reference spectrum were superposed directly on the stellar spectrum prior to the starlight entering the spectrograph. This idea has been used by a number of groups, including Marcy & Butler (1922) and Butler et al. (1996b). The wavelengths of lines used for radial velocity measurements in Paper I were measured relative to iodine absorption lines, produced by an iodine cell. The cell is mounted directly in front of the entrance slit of the spectrograph. Other groups have used either similar chemical absorption cells, telluric lines, or Fabry-Perot interferometers to provide a reference spectrum (Griffin & Griffin 1973b; Campbell 1983; McMillan et al. 1993; Cochran et al. 1991).

The observations reported in this paper were taken at Lick Observatory from 1990 August 14 to 1990 September 1, using the 0.6 m Coudé Auxiliary Telescope (CAT) and the "Hamilton" coudé echelle spectrometer (Vogt 1987). Further details about these observations can be found in Table 3 of Paper I, which presents precise radial velocity measurements for the wavelength region between 5000 and 6300 Å. However, the strength of molecular iodine lines steadily diminishes as wavelength increases, and above 6300 Å iodine lines cannot be used. For this paper, telluric lines (primarily due to water vapor) in the near-IR have been used to provide a fiducial wavelength scale against which to measure radial velocities.

Approximately 100 near-IR (8000 Å) stellar lines were identified in each of the three stars using a program which generates synthetic spectra (Bell 1973), and the US NBS solar wavelength table (Moore, Minnaert, & Houtgast 1966). Figure 1 shows the spectrum of a typical echelle order for η Aql. A synthetic stellar spectrum and a telluric spectrum are also shown, the latter being computed using the SAAG3 program (Stevenson 1994).

The "pixel" position of lines in the Cepheid spectra were determined with the 0.7 line bisector method (Kulander & Jefferies 1966; Paper I). Wavelengths were assigned to pixels based on the position of the embedded telluric water vapor lines. These lines are easily distinguished from stellar lines because of their extreme narrowness. A reference telluric spectrum was obtained by observing the rapidly rotating late O star HR 8154. The few absorption lines in the spectrum of a normal O star are rotationally broadened out of the spectrum of HR 8154, yielding an essentially featureless spectrum. This star thus serves as an incandescent lamp upon which the "telluric" absorption spectrum of Earth's atmosphere is impressed.

3. A COMPARISON OF IR AND VISIBLE RADIAL VELOCITY CURVES

Sasselov et al. (1989) and Sasselov & Lester (1990) have suggested that Cepheid radial velocity amplitudes from 1.1 μm lines are 20%–35% larger than those derived from visible spectra. A preliminary investigation of this problem,

using lines over a relatively small wavelength interval, was carried out using synthetic Cepheid spectra (Paper II, Fig. 12). The inclusion of velocity gradients in the model resulted in the amplitude of the radial velocity curve from strong high EP Fe I lines near 6000 Å being about 1 km s^{-1} larger than that from a similar set of Fe I lines near 5000 Å (a 2.5% effect). Models constructed without such gradients did not show similar significant radial velocity differences.

In Paper I (Table 5) precise radial velocity curves were constructed for several groups of lines in the visible. Matching sets of lines have been found in the near-IR and are listed in Table 1. The differences in radial velocity between the near-IR and visible lines are shown for the three program stars in Figures 2, 3, and 4.

The results for the Cepheid prototype δ Cep are shown in Figure 2. The standard Fe I radial velocity curve (found

TABLE 1
ABSORPTION LINES USED IN VELOCITY ANALYSIS

Atom	λ	EP (eV)	δ Cep	η Aql	X Cyg
Fe I	6408.00	3.69	X	X	X
Fe I	6411.63	3.65	X	X	X
Fe I	6419.93	4.73	X	X	X
Fe I	6569.20	4.73	X	X	X
Fe I	6705.08	4.61	X
Fe I	7130.89	4.22	X	X	X
Fe I	7386.30	4.91	X
Fe I	7411.12	4.28	X	...	X
Fe I	7418.63	4.41	X
Fe I	7495.04	4.22	...	X	...
Fe I	7510.99	4.18	...	X	...
Fe I	7807.87	4.99	X
Fe I	7937.11	4.31	...	X	...
Fe I	8046.02	4.41	X
Fe II	6416.90	3.89	X	X	X
Fe II	7515.79	3.90	...	X	...
Fe II	7711.69	3.90	...	X	X
Ca I	5581.96	2.52	X
Ca I	5588.74	2.52	X	X	X
Ca I	5590.10	2.52	X	X	X
Ca I	5594.45	2.52	X
Ca I	5598.47	2.52	X	...	X
Ca I	5601.27	2.52	X	...	X
Ca I	6471.64	2.52	X	X	...
Ca I	6493.76	2.52	X	...	X
Ca I	6717.66	2.71	X	X	...
Ca I	7326.12	2.93	X
Ni I	5082.35	3.65	X	X	X
Ni I	5084.07	3.67	X
Ni I	5176.55	3.89	X	X	X
Ni I	5694.96	4.08	X	...	X
Ni I	5715.05	4.08	X	X	X
Ni I	5760.81	4.10	X
Ni I	5996.72	4.23	X
Ni I	6116.16	4.08	X
Ni I	6183.83	4.16	X
Ni I	6186.70	4.10	X
Ni I	6204.58	4.09	X
Ni I	6772.29	3.66	X	X	X
Ni I	7122.17	3.54	X	X	X
Ni I	7393.57	3.61	X	X	X
Ni I	7422.25	3.63	X	X	X
Ni I	7797.55	3.90	X	X	X
Fe I	6393.58	2.43	X	X	X
Fe I	6945.17	2.42	...	X	X
Fe I	8047.02	0.86	...	X	X
Fe I	8387.73	2.18	X
Fe I	8401.36	2.48	X
Fe I	8514.00	2.19	X	X	X
Y II	6795.40	1.73	X	X	X

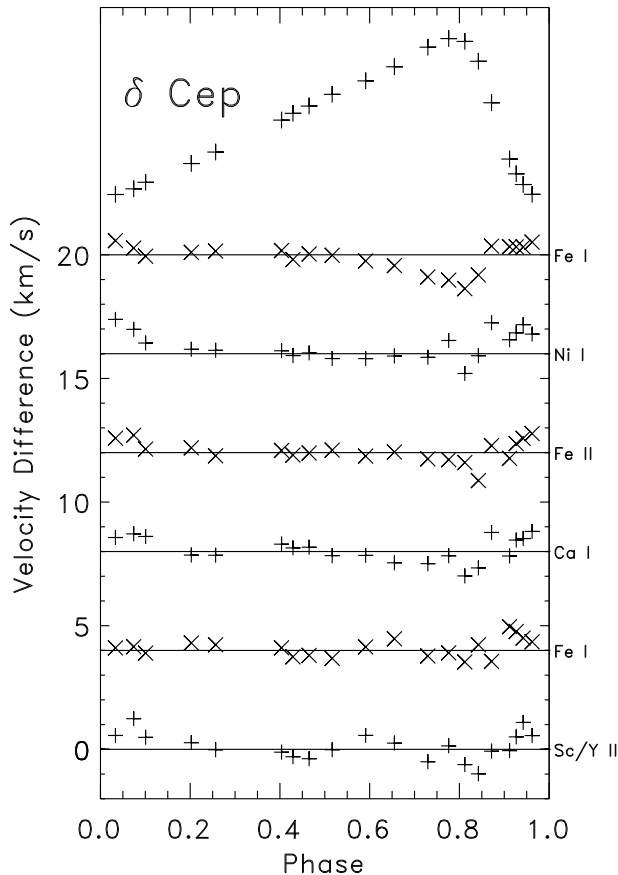


FIG. 2.—Comparison of near-IR and visible radial velocity curves for δ Cep. The “standard” radial velocity curve of δ Cep is shown at top (and Fig. 3 of Paper I). The differences between the near-IR and visible radial velocity curves are shown for several groups of lines. These line groups are indicated along the right edge of the figure. The Fe I lines at the top of the figure are from high-EP lines, while Fe I lines near the bottom of the figure are for low-EP lines. The visible lines are listed in Table 1 of this paper and Table 5 of Paper I. The near-IR lines are listed in Table 1 of this paper. An arbitrary offset has been added to each of the line sets.

from the 3–6 eV Fe I lines) is shown at the top of the figure. The classes of lines are indicated along the right edge of the figure. The Fe I lines indicated near the bottom figure are from low EP lines, while the Fe I near the top of the figure are from high EP lines. The radial velocity differences are less than 1 km s^{-1} for all of the visible/near-IR comparisons.

The results for η Aql are shown in Figure 3. Again, no significant radial velocity differences between the visible and near-IR lines are seen in this star.

Figure 4 shows the results for the long-period Cepheid X Cyg. Radial velocity differences are seen in the lines of Ni I, Ca I, Sc II, and Y II, with the IR lines having a larger amplitude by typically 3 km s^{-1} . In contrast, the low-EP lines of Fe I have a smaller amplitude in the near-IR by about 3 km s^{-1} . The high-EP lines of Fe I and lines of Fe II have similar velocity curves in both the visible and near-IR.

Calculations of continuum optical depths for a Cepheid model atmosphere with $T_{\text{eff}} = 6000 \text{ K}$, $\log g = 1.5$, and solar abundances show that Rayleigh scattering by atomic hydrogen is an important opacity source near the surface at shorter wavelengths (i.e., 5000 \AA) and H^- is dominant elsewhere. The wavelength dependence of the H^- opacity affect the physical depth at which metal lines are formed. At the

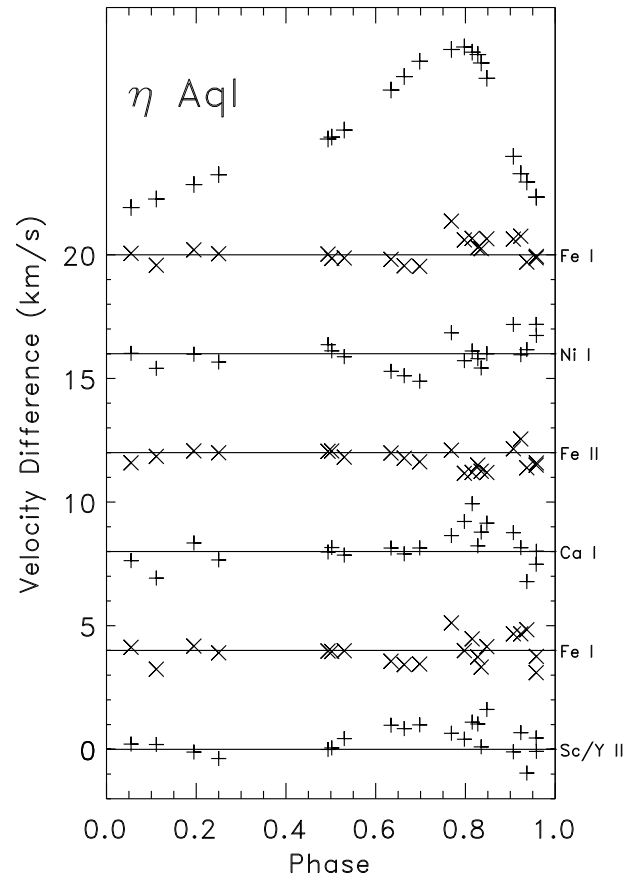


FIG. 3.—Same as Fig. 2 for η Aql. The standard high-EP Fe I velocity curve is shown at top and in Fig. 8.

same physical depths where $\tau(5000 \text{ \AA}) = 0.01122$ and 0.12589 , the optical depth of $\tau(8000 \text{ \AA})$ are 0.01066 and 0.15050 , and those of $\tau(11000 \text{ \AA})$ are 0.00854 and 0.12124 . Thus the effect of a velocity gradient on strong lines will be similar at 5000 \AA and 8000 \AA , but lines at 11000 \AA might be expected to show radial velocity and line profile differences, including line splitting. Conversely, weak lines formed at 5000 \AA and 11000 \AA will be similarly affected by a velocity gradient, but those at 8000 \AA would differ. The lines used in this study are systematically the strongest lines, consistent with our small observed differences in radial velocity between lines at 5000 \AA and 8000 \AA . It is very difficult to precisely measure the radial velocities of weak lines, but further studies should consider this problem. Future studies of velocity gradients in Cepheid atmospheres should be made using lines with a wide range of wavelengths.

The only star in common between this study and that of Sasselov et al. (1989) is η Aql. Their 11000 \AA radial velocity curve for η Aql agrees with the standard visible Fe I curve of Paper I to within about 1 km s^{-1} , which is within the errors, and which contradicts their suggestion of differences. The greater splitting of the hydrogen lines seen in longer period stars might lead to observable differences in these objects.

4. H α AND H β

Several investigators have studied Cepheid H α line profiles and radial velocity curves (Grenfell & Wallerstein 1969; Wallerstein 1972, 1979; Jacobsen & Wallerstein 1982; Wallerstein et al. 1992; Breittellner & Gillet 1993a, 1993b,

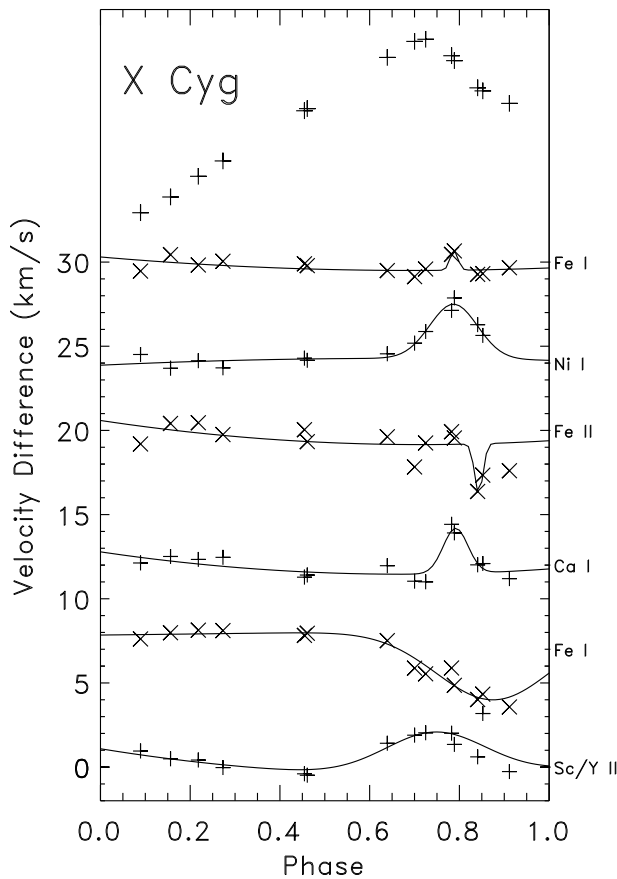


FIG. 4.—Same as Fig. 2 for X Cyg. The standard high-EP Fe I velocity curve is shown at top and in Fig. 11.

1993c). H β has not been as extensively studied.

Figure 5 presents the H α and H β radial velocity curves (determined by the 0.7 bisector) for δ Cep. For comparison, the “standard” Fe I radial velocity curve is also shown. (Radial velocities from H α , H β , and Fe I for δ Cep, η Aql, and X Cyg are given in Table 2.) The full amplitude of the H α radial velocity curve is 52.5 km s $^{-1}$, or 34% greater than the Fe I velocity curve. This is in excellent agreement with Wallerstein (1979), who found the H α amplitude to be 53

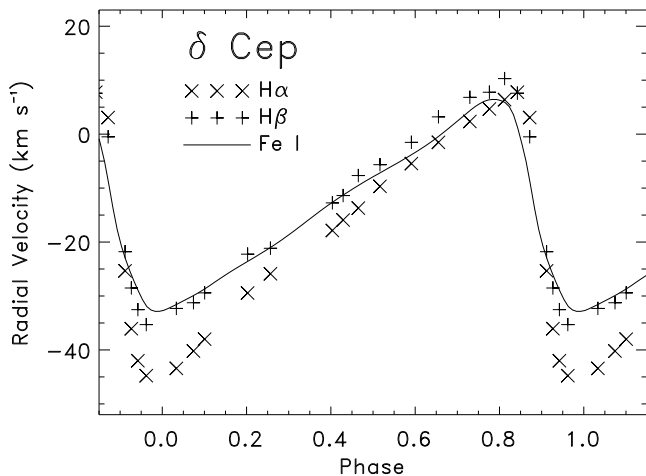


FIG. 5.—Radial velocity curves from H α (cross), H β (plus), and the high-EP lines of Fe I (solid line) for δ Cep. The amplitude of the H α RV curve is 34% greater than the standard Fe I RV curve. Both the H α and H β velocity curves appear continuous, particularly near maximum infall velocity.

TABLE 2
RADIAL VELOCITIES FROM H α , H β , AND Fe I

Star	Heliocentric (JD + 2,440,000)	Phase	Fe I Velocity (km s $^{-1}$)	H β Velocity (km s $^{-1}$)	H α Velocity (km s $^{-1}$)
δ Cep ...	8117.993	828.100	-28.34	-29.42	-38.00
	8119.949	828.465	-9.84	-7.68	-13.71
	8120.969	828.655	-0.28	3.20	-1.53
	8121.811	828.812	5.86	10.29	6.39
	8123.906	829.202	-23.77	-22.25	-29.45
	8124.985	829.403	-13.22	-12.74	-17.86
	8125.991	829.591	-3.68	-1.52	-5.46
	8126.735	829.729	4.47	6.82	2.35
	8126.984	829.776	6.56	7.76	4.66
	8127.712	829.911	-22.66	-21.79	-25.34
	8127.792	829.926	-26.26	-28.52	-36.06
	8127.875	829.942	-28.86	-32.53	-42.00
	8127.982	829.962	-31.23	-35.30	-44.77
	8130.957	830.516	-7.01	-5.66	-9.67
	8132.706	830.842	1.04	7.58	7.77
	8132.863	830.871	-8.99	-0.50	3.07
	8133.731	831.033	-31.29	-32.31	-43.42
	8133.949	831.074	-29.94	-31.25	-40.20
8134.929	831.256	-20.97	-21.16	-25.89	
8135.854	831.429	-11.58	-11.38	-15.92	
η Aql....	8117.822	661.698	6.96	5.52	-5.16
	8118.752	661.827	8.60	17.78	15.82
	8118.806	661.835	6.55	17.96	17.05
	8118.896	661.847	2.83	17.45	18.64
	8119.686	661.957	-25.97	-27.59	-28.61
	8120.786	662.111	-26.46	-26.61	-39.22
	8121.784	662.250	-20.57	-20.60	-27.87
	8123.792	662.529	-9.74	-7.21	-10.96
	8124.751	662.663	3.25	0.14	-8.89
	8125.713	662.797	10.43	15.40	11.00
	8125.838	662.815	9.16	17.05	14.36
	8126.712	662.936	-22.34	-19.26	-0.00
	8126.866	662.958	-26.05	-25.27	-26.29
	8130.710	663.493	-11.90	-8.33	-11.94
	8130.769	663.502	-11.44	-6.87	-11.56
	8131.717	663.634	-0.03	-3.05	-10.47
	8132.683	663.768	9.82	12.58	7.62
	8133.674	663.906	-16.12	-7.14	2.98
8133.793	663.923	-20.32	-14.34	0.00	
8134.736	664.054	-28.53	-31.78	-43.95	
8135.741	664.194	-22.96	-22.38	-31.44	
X Cyg...	8118.845	245.724	36.33	33.35	10.45
	8119.791	245.782	31.59	41.20	32.41
	8119.895	245.788	30.06	41.33	31.81
	8120.744	245.840	21.57	41.89	36.51
	8120.933	245.852	20.70	43.40	36.77
	8121.905	245.911	17.29	33.02	10.45
	8124.819	246.089	-15.42	-11.67	32.48
	8125.914	246.156	-10.62	-9.68	27.03
	8126.930	246.218	-4.59	-5.69	22.26
	8127.829	246.273	-0.02	-5.34	18.53
	8130.805	246.454	15.05	9.74	7.25
	8130.909	246.460	15.68	10.74	6.44
8133.831	246.639	30.73	22.62	6.32	
8134.827	246.700	35.74	30.40	5.90	

km s $^{-1}$. Wallerstein found that the maximum infall velocity of the H α line exceeded that from the “metallic” lines by 10 km s $^{-1}$, while Figure 5 here shows a difference of only a few km s $^{-1}$. At maximum infall velocity, the H α velocity curve presented here appears more continuous than Wallerstein found. The H α velocity curve lags the Fe I curve by 0.05 in phase.

In contrast, the H β velocity curve follows the Fe I curve much more closely, being only 16% larger in amplitude, and showing a smaller (0.03) phase lag. The profiles of both the H α and H β lines are smooth and continuous at all phases, as shown in Figures 6 and 7.

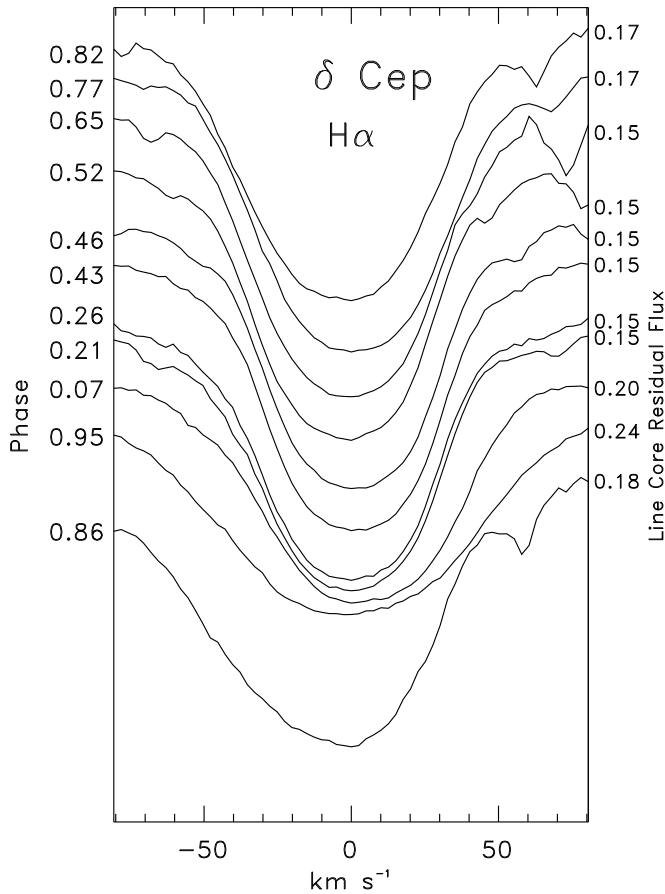


FIG. 6.— $H\alpha$ line profiles as a function of phase for δ Cep. The profiles have been shifted horizontally so that the line core minima are centered at 0 km s^{-1} . The profiles have also been shifted vertically by an arbitrary amount. The profiles remain relatively symmetric at all phases. The line width increases at maximum infall velocity.

The $H\alpha$, $H\beta$, and “standard” Fe I radial velocity curves for η Aql are shown in Figure 8. The amplitude of the $H\alpha$ velocity curve is 57% larger than that from the Fe I lines. The $H\alpha$ amplitude is 62.5 km s^{-1} , somewhat different from the 67 km s^{-1} shown in Figure 1 of Jacobsen & Wallerstein (1981). There is also some question about the velocity zero point between the standard Fe I lines and $H\alpha$. Jacobsen & Wallerstein found the $H\alpha$ velocity curve generally followed the Fe I velocity curve from phase 0.0 through 0.8, while we find that at maximum infall velocity, the $H\alpha$ curve lags the Fe I lines by 0.07 in phase.

The amplitude of the $H\beta$ radial velocity curve is 25% larger than the Fe I curve. The $H\beta$ curve is seen to generally follow the Fe I curve, deviating only at maximum infall velocity where it instead follows the $H\alpha$ curve.

Figures 9 and 10 show the $H\alpha$ and $H\beta$ line profiles as a function of phase for η Aql. The $H\alpha$ line is relatively symmetric throughout most of the pulsation cycle, but just after maximum infall velocity the profiles become wildly asymmetric. The hint of line doubling seen in Figure 3 of Jacobsen & Wallerstein (phase 0.94) is not seen here. In contrast, the $H\beta$ line remains symmetric at all phases, though it does become much broader just after maximum infall velocity.

The $H\alpha$, $H\beta$, and “standard” Fe I radial velocity curves for X Cyg are shown in Figure 11. The amplitude of the $H\beta$ velocity curve generally follows the standard Fe I curve. Its

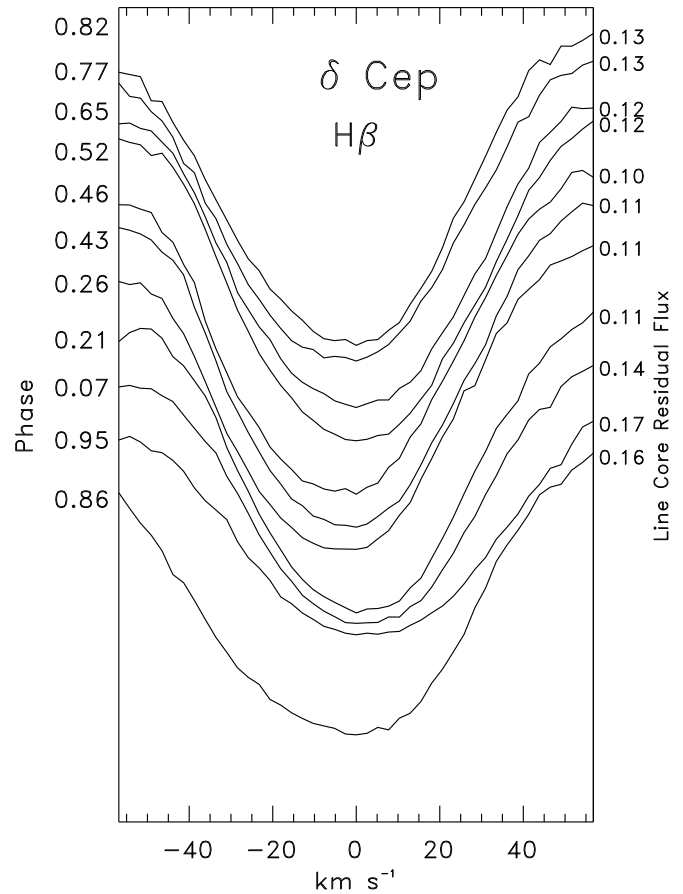


FIG. 7.— $H\beta$ line profiles as a function of phase for δ Cep. The profiles are relatively symmetric at all phases.

amplitude is only 6% larger, and it lags in phase by 0.12. The extreme line doubling of $H\alpha$ seen in X Cyg (Fig. 12) renders any attempt to measure a single radial velocity subject to considerable interpretation. For this case, a 0.7 bisector was blindly applied. For the phases when the sec-

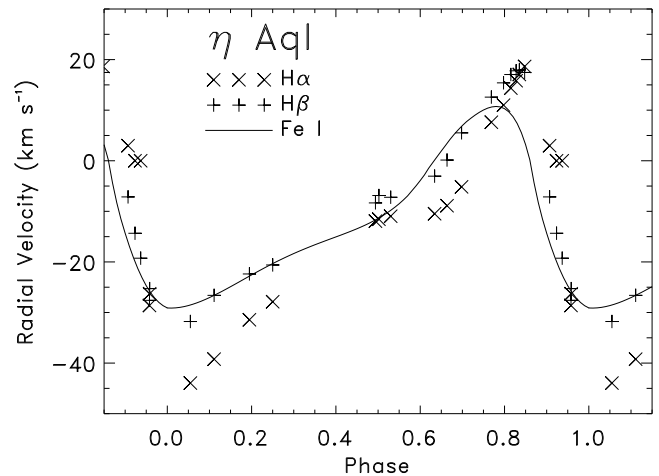


FIG. 8.—Radial velocity curves from $H\alpha$, $H\beta$, and the high-EP lines of Fe I for η Aql. The $H\alpha$ and $H\beta$ velocity amplitudes are larger by 57% and 25%, respectively, compared to the Fe I velocity curve. Both the $H\alpha$ and $H\beta$ velocity curves exhibit a lag of 0.07 in phase relative to Fe I, and both H velocity curves appear nearly discontinuous near maximum infall velocity. The RV curve of $H\beta$ follows the Fe I RV curve closely for most of the cycle, but it follows the $H\alpha$ RV curve near maximum infall velocity.

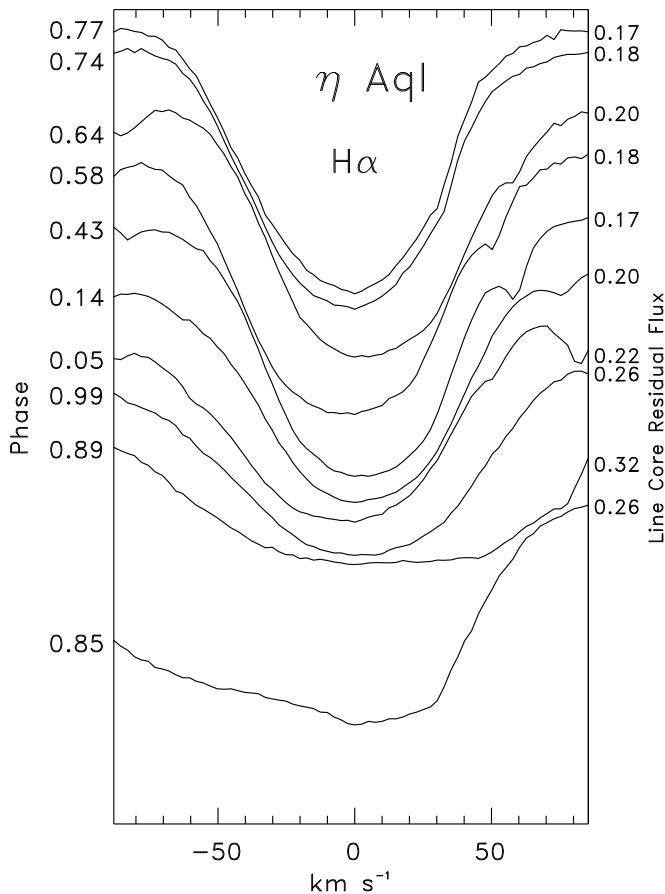


FIG. 9.—H α line profiles as a function of phase for η Aql, shifted vertically by an arbitrary amount. The profiles become extremely asymmetrically “distorted” just after maximum infall velocity.

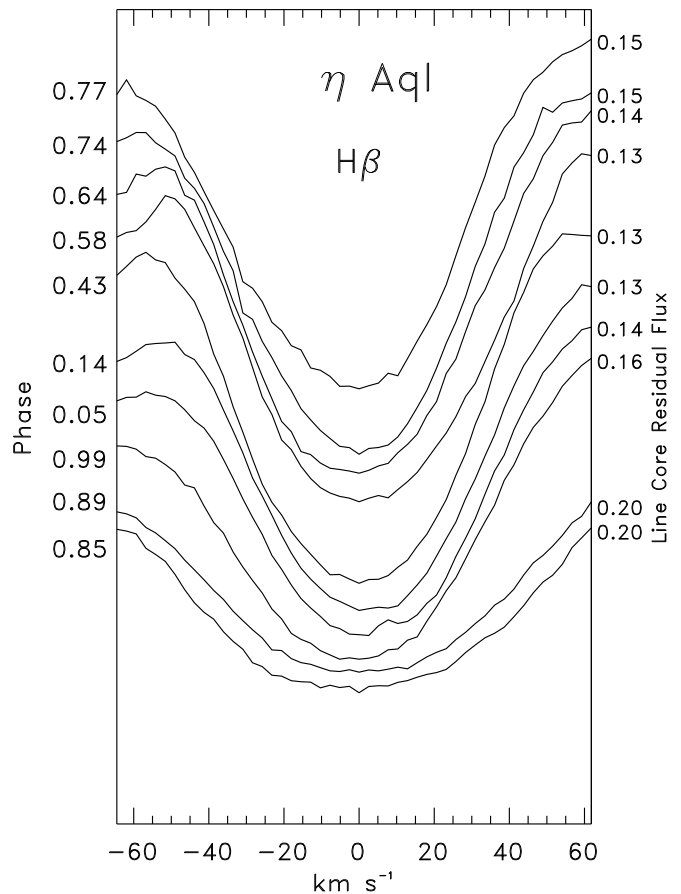


FIG. 10.—H β line profiles as a function of phase for η Aql. The profiles are relatively symmetric at all phases.

ondary line component is weak this then finds the bisector about the primary component. When the secondary component is nearly as deep as the primary, the bisector is found about the combined and secondary components. As Figure 11 shows, the derived H α velocity curve is completely out of phase with that from the Fe I lines. This behavior has been previously noted by Kraft (1960) and Wallerstein (1983). However, the radial velocity amplitude of the H α line in Figure 11 is significantly smaller than that shown by Wallerstein (1983, Fig. 1). This difference is probably due to the ambiguities in measuring the line position of a line that shows extreme asymmetries and outright doubling.

Figures 12 and 13 show the line profiles of H α and H β for X Cyg. The H α line is doubled for over half the pulsation cycle, from phase 0.70 through 0.27. This behavior has been discussed at length by Wallerstein (1983). Unlike the shorter period Cepheids, the H β profile in X Cyg undergoes extreme asymmetries, and even incipient line doubling from phases 0.09 through 0.15.

5. LINE PROFILE ASYMMETRIES

As Paper I (Fig. 7) demonstrates, Cepheid radial velocity curves are strongly influenced by the method used to measure line positions. The various measurement techniques give different results because Cepheid absorption lines are subject to extreme and rapidly changing asymmetries as a function of pulsation phase.

In order to characterize line profile asymmetries, Sasselov & Lester (1990) have defined an asymmetry parameter to describe the strength and direction of a line asymmetry. The position of the line core minimum is found by a parabolic fit to the three lowest points in the line. The location of the left and right half-height (midway between the continuum and

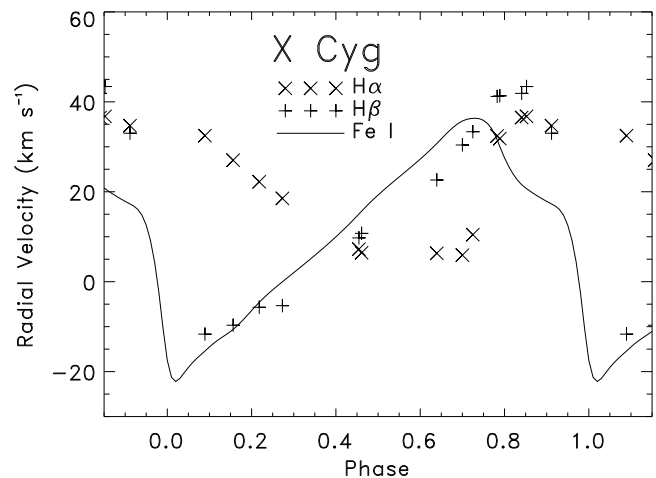


FIG. 11.—Radial velocity curves from H α , H β , and the high-EP lines of Fe I for X Cyg. The H β velocity curve roughly follows that of the Fe I velocities. Its amplitude is larger by 6% and it lags in phase by 0.12 cycles. In contrast, the behavior of the H α velocity curve is quite bizarre, falling during the rising branch of the Fe I velocity curve, and then abruptly rising during the falling branch of the Fe I curve.

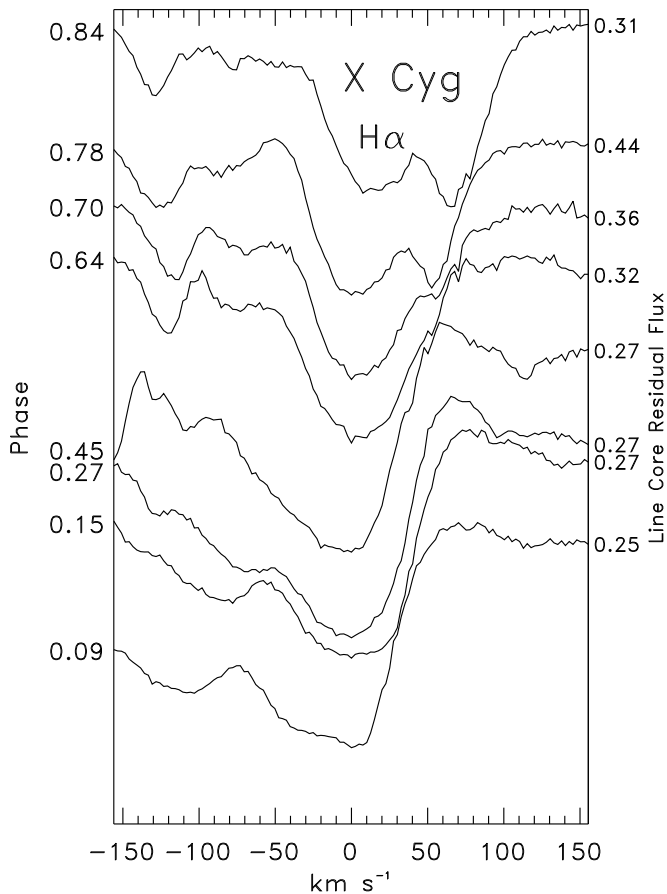


FIG. 12.— $H\alpha$ line profiles as a function of phase for X Cyg. The line splits into two components just before the phase of maximum infall velocity. This line doubling persists for as much as half a pulsation period.

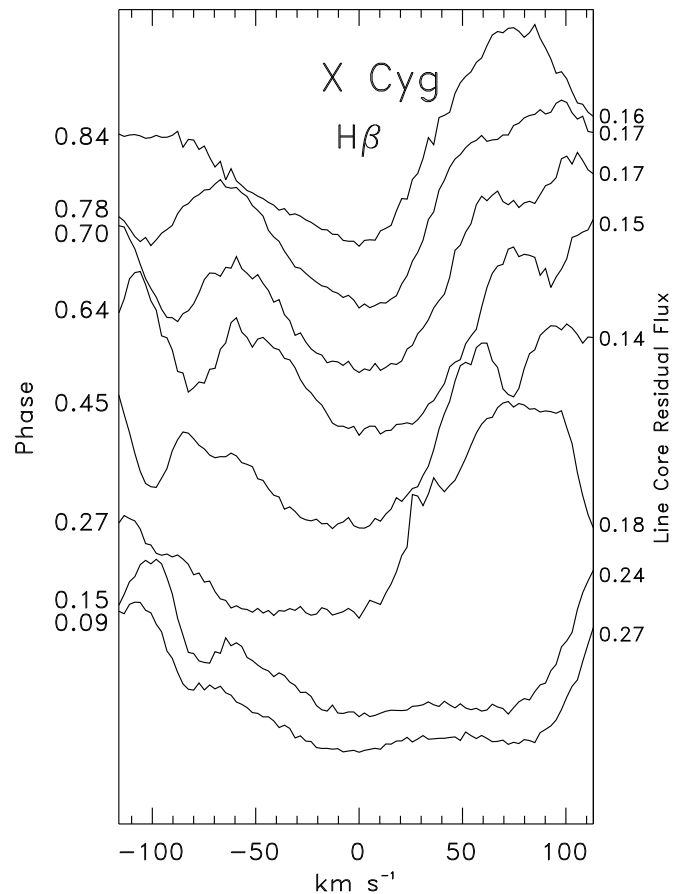


FIG. 13.— $H\beta$ line profiles as a function of phase for X Cyg. Extreme asymmetries develop in the line profile just before maximum infall velocity. Weak evidence of line doubling is seen near phase 0.1.

the core) of the line is found by linear interpolation. The asymmetry parameter is given by the log of the ratio of the left half-width to the right half-width.

Figure 14 shows the asymmetry parameter, derived from the near-IR lines, as a function of phase for each of the program stars. The crosses indicate the asymmetry parameter for the high-EP lines (Fe I, Fe II, Si I, and Mg I), while the diamonds represent the low-EP Fe I and Y II lines. All the lines follow a pattern of maximum left asymmetry near phase 0.0 and maximum right asymmetry near phase 0.8. The maximum left asymmetry is similar for all the lines, but the maximum right asymmetry for the high-EP lines is greater than for the low-EP lines. The maximum right asymmetry for the high-EP lines in the two larger amplitude Cepheids, η Aql and X Cyg, is significantly greater than that for δ Cep. These results are very similar to those derived from the visible lines in Paper I. It is during the phase of maximum rightward asymmetry that the larger amplitude Cepheids cross from the hot to the cool side of the granulation boundary, as denoted by a reversal in the shape of line bisectors (Gray & Nagel 1989).

Breitfellner & Gillet (1993c) report observing true inverse P Cygni profiles near 5860 and 5920 Å at phase 0.458 for X Cyg. Figure 15 shows the spectrum of X Cyg, also observed at phase 0.458, which was taken (see Table 2, Paper I) approximately 1 yr after that of Breitfellner & Gillet. This figure is quite similar to Figure 3 of Breitfellner & Gillet (1993c), both in resolution and wavelength cover-

age, but no evidence of inverse P Cygni profiles is seen, in particular at 5864 Å. In all other respects, such as line depths and the doubling of the Na lines (due to the interstellar component), the two figures are nearly identical.

Breitfellner & Gillet (1993a) also reported observing P Cygni type emission for η Aql. As discussed in Paper II (Fig. 4), this behavior was not observed at a similar phase in spectra taken a year after the Breitfellner & Gillet data.

Kraft (1956) reported observing line doubling in a small number of blue low-EP lines in one spectrum of X Cyg, though this behavior has not been seen by subsequent observers. Arguing on the basis of bumps in calculated opacities averaged over 100 Å intervals, Sasselov & Lester (1990) suggested that line splitting might be observed near 5300 and 6100 Å. However, it is not clear that the effects of numerous spectral lines, combined into opacity distribution functions, will correspond to changes in the continuous opacity for this particular problem. With the exception of the Balmer lines, there are no unambiguous examples of line splitting in the region of 4800 Å–8500 Å for any of the three program stars presented here.

6. DISCUSSION

The overall behavior of the near-IR lines is very similar to that of the visible lines. They produce similar radial velocity results and very similar line profile asymmetries.

The data presented here suggest a progression: δ Cep has the shortest period (5 days), shows no radial velocity differ-

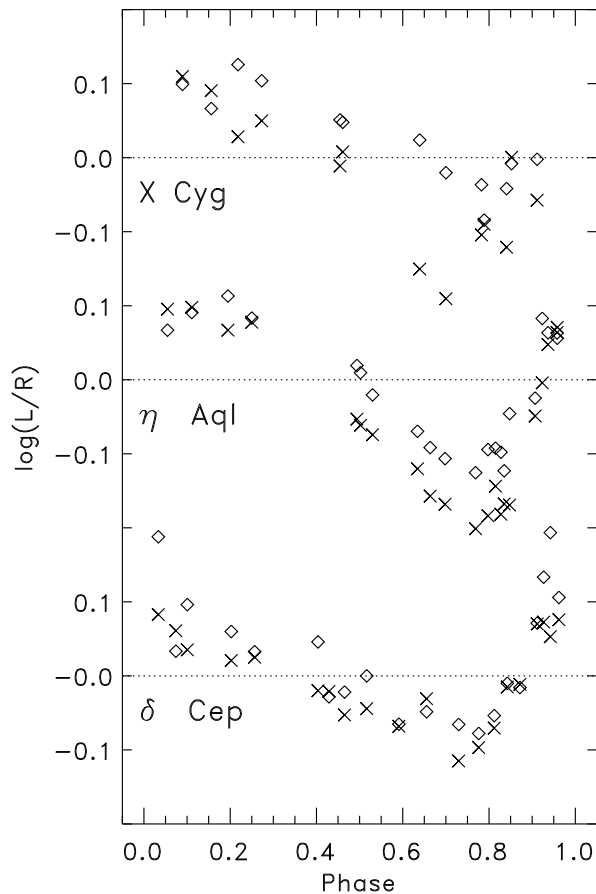


FIG. 14.—The near-IR Sasselov-Lester asymmetry parameter for each of the program stars. It is formed by taking the logarithm of the left-to-right half-width ratio of line profiles. Symmetric line profiles have a value of zero. Negative values indicate a blue extended line wing, positive for a red extended wing. The crosses represent the asymmetry for the standard high-EP Fe I lines. The diamonds represent the lines of Sc II, Y II, Fe II, and the low-EP lines of Fe I.

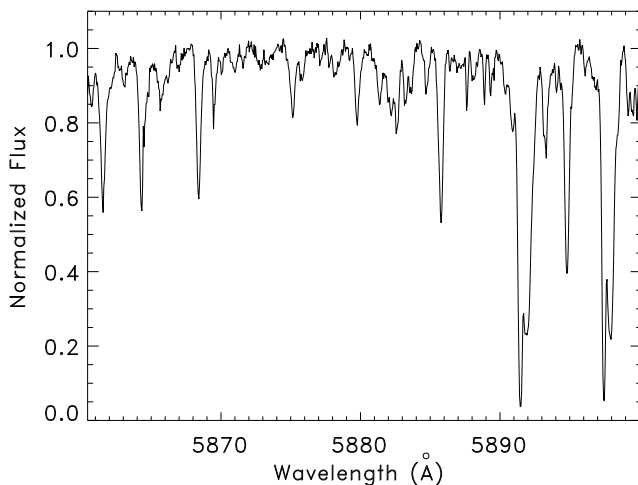


FIG. 15.—One order of the X Cyg spectrum observed 1990 August 27 at phase 0.458. Breitfellner & Gillet (1993c) reported observing true inverse P Cygni profiles in this wavelength region at phase 0.458, but no evidence of P Cygni profiles is seen here. The weak extremely narrow lines near 5890 Å are due to telluric water vapor.

ences as a function of wavelength, and only a small radial velocity difference from lines of different excitation (Paper I). There is a very slight “hump” on the rising branch of the radial velocity curve. The $H\alpha$ and $H\beta$ radial velocity curves are continuous, and only slightly different than the “standard” Fe I radial velocity curve. Line profile asymmetries are relatively small. The asymmetries of low- and high-EP lines are similar.

η Aql has a slightly longer period (7 days). It still does not show significant radial velocity differences as a function of wavelength. It does have stronger radial velocity differences for lines of different excitation. The “hump” on the rising branch of the radial velocity curve is more pronounced. The $H\alpha$ and $H\beta$ curves have a significantly larger amplitude than the standard Fe I radial velocity curve, and the $H\alpha$ curve appears discontinuous at maximum infall velocity. Line asymmetries are larger, and the low-EP and high-EP lines have different “asymmetry amplitudes.”

X Cyg has the longest period (16 days) in this study. It shows some wavelength-dependent radial velocity differences. It has significant radial velocity differences for lines of different excitation. There is a strong “hump” (almost a shelf) on the steeply descending branch of the radial velocity curve. The amplitude of the $H\alpha$ radial velocity curve is completely out of phase with the “standard” Fe I radial velocity curve. The $H\alpha$ line is flagrantly split for half the pulsation cycle, while the $H\beta$ line shows incipient splitting at the phase of maximum infall velocity.

Our discussion of the velocity differences between lines of different excitation and/or species is based on the inclusion of radial velocity gradients in a model Cepheid photosphere. However, such effects are commonly seen in non-pulsating stars. Gray & Nagel (1989) have shown that spectral line bisectors differ on either side of a granulation boundary, which occurs at spectral type G1 for Ib supergiants. Their line asymmetries correspond to velocity differences of a few km s^{-1} . The longer period Cepheids will cross this boundary. Since the phenomena occurring in static stars will also presumably occur in pulsating stars, the interpretation of Cepheid velocity curves becomes more complex.

As shown earlier, the inclusion of velocity gradients in Cepheid atmospheres introduces constraints on the relationship between radial velocity curves and pulsational velocity. The velocity gradient used in Paper II predicted a velocity difference of 1 km s^{-1} between lines in the 5000 and 6000 Å regions. No such difference was observed between lines at 5000 Å and 8000 Å, and a comparison between an 11000 Å curve and the standard curve of Paper I did not confirm a proposed difference. It is clearly necessary to obtain radial velocity curves over a broad wavelength interval to understand the relationship between radial and pulsational velocity. In particular, precision radial velocity measurements near 11000 Å, using either an absorption cell or telluric lines as a wavelength metric, would be extremely useful. It is extremely important to properly account for atmospheric velocity gradients in the derivation of the pulsational velocity from the radial velocity. The gradient included in Paper II altered the M_V derived for η Aql by the Barnes-Evans method by 0.4 mag.

The propagation of progressive waves and shocks through the radiative atmosphere of a Cepheid is a complicated phenomenon (Wallerstein & Elgar 1992). As Sasselov & Lester (1990) point out, maximum Cepheid pulsational

velocities are typically more than triple the sound speed, suggesting the appearance of shock waves. This is further supported by some observations of metal line splitting in η Aql (Sasselov et al. 1989) and X Cyg (Kraft 1956), although our data do not support these observations, and in W Vir (Sanford 1952) as well as by hydrogen line splitting. The propagation of the wave is made even more difficult by radiative transfer in a non-LTE environment. The proper interpretation of spectroscopic data will require a full-scale hydrodynamic, non-LTE, radiative transfer model of a pulsating atmosphere with propagating shocks (Sasselov & Lester 1990; Jacobsen & Wallerstein 1981). Recent advances in computational hardware and software should make this possible in the next few years (Sasselov & Raga 1992). The BE/BW problem will finally be solved when such a model is able to match observed details of high-resolution Cepheid spectra.

Many of the problems associated with BE/BW distance determinations of normal amplitude Cepheids, such as shocks, photospheric velocity gradients, and extreme line asymmetries, are minimized for the case of short-period, small-amplitude Cepheids. Such Cepheids typically have periods of 4 days or less, amplitudes of 10 km s^{-1} or less, and sinusoidal radial velocity curves (Eggen 1985). A representative case, FF Aql, did not show significant line profile or radial velocity variations as a function of atomic ioniza-

tion or excitation level, suggesting that strong atmospheric velocity gradients do not form (Paper I). Based on the results of this paper, it is further expected that such stars do not have line profiles or radial velocity curves with a significant wavelength dependence. While BE/BW distances for normal amplitude stars are strongly model-dependent and currently have uncertainties of 10%–20% (Paper II), derived distances for small-amplitude Cepheids should in principle be more precise and easier to calculate. Since standard radial velocity measurement techniques have errors of 1 km s^{-1} or more, it is important to determine the radial velocity curves of small-amplitude Cepheids with one of the newer precision velocity techniques (Paper I), otherwise 10% errors will be introduced into the radial velocity curves.

Such observations of short-period Cepheids should yield accurate BE/BW absolute magnitudes for them, thereby calibrating the zero point of the Cepheid P - L relationship, with the slope being found from the Magellanic Cloud Cepheids.

The anonymous, and courteous, referee made several helpful comments, one leading to the last two paragraphs of the paper. R. P. B. and R. A. B. acknowledge the support of NASA grant NAGW-3182 and NSF grant AST 93-14931, respectively.

REFERENCES

- Albrow, M. D., & Cottrell, P. L. 1994, *MNRAS*, 267, 548
 Barnes, T. G., & Evans, D. S. 1976, *MNRAS*, 174, 489
 Barnes, T. G., Dominy, J. F., Evans, D. S., Kelton, P. W., Parsons, S. B., & Stover, R. J. 1977, *MNRAS*, 178, 661
 Bell, R. A. 1973, *MNRAS*, 164, 197
 Böhm-Vitense, E., Garnavich, P., Lawler, M., Mena-Werth, J., Margan, S., Peterson, E., & Temple, S. 1989, *ApJ*, 343, 351
 Breitfellner, M. G., & Gillet, D. 1993a, *A&A*, 277, 524
 ———. 1993b, *A&A*, 277, 541
 ———. 1993c, *A&A*, 277, 553
 Butler, R. P. 1993, *ApJ*, 415, 323 (Paper I)
 Butler, R. P., Bell, R. A., & Hindsley, R. B. 1996a, *ApJ*, 461, 362 (Paper II)
 Butler, R. P., Marcy, G. W., Williams, E., McCarthy, C., Dosanjh, P., & Vogt, S. S. 1996b, *PASP*, 108, 500
 Campbell, B. 1983, *PASP*, 95, 577
 Cochran, W. D., Hatzes, A. P., & Hancock, T. J. 1991, *ApJ*, 380, L35
 Dravins, D. 1995, in *IAU Symp. 176, Stellar Surface Structure*, ed. K. G. Strassmeier & J. L. Linsky (Dordrecht: Kluwer), 519
 Eggen, O. J. 1985, *AJ*, 90, 1278
 Evans, N. R. 1984, *ApJ*, 281, 760
 Fernie, J. D. 1984, *ApJ*, 282, 641
 Freedman, W. L., et al. 1994, *ApJ*, 427, 628
 Gieren, W., & Fouqué, P. 1993, *AJ*, 106, 734
 Gray, D. F., & Nagel, T. 1989, *ApJ*, 341, 421
 Grenfell, T. C., & Wallerstein, G. 1969, *PASP*, 81, 732
 Griffin, R., & Griffin, R. 1973a, *MNRAS*, 162, 243
 ———. 1973b, *MNRAS*, 162, 255
 Jacobsen, T. S., & Wallerstein, G. 1981, *PASP*, 93, 481
 Kraft, R. P. 1956, *PASP*, 68, 137
 ———. 1960, in *Stellar Atmospheres*, ed. J. L. Greenstein, (Chicago: Univ. Chicago Press), 370
 Kulander, J. L., & Jefferies, J. T. 1966, *ApJ*, 146, 194
 Marcy, G. W., & Butler, R. P. 1992, *PASP*, 104, 270
 McMillan, R. S., Moore, T. L., Perry, M. L., & Smith, P. H. 1992, *ApJ*, 403, 801
 Moore, C. E., Minnaert, M., & Houtgast, J. 1966, *NBS Monog.* 61
 Sanford, R. F. 1952, *ApJ*, 116, 331
 ———. 1956, *ApJ*, 123, 201
 Sasselov, D. D., & Karovska, M. 1994, *ApJ*, 432, 367
 Sasselov, D. D., & Lester, J. B. 1990, *ApJ*, 362, 333
 Sasselov, D. D., Lester, J. B., & Fieldus, M. S. 1989, *ApJ*, 337, L29
 Sasselov, D. D., & Raga, A. 1992, in *Cool Stars, Stellar Systems, and the Sun*, ed. M. S. Giampapa & J. A. Bookbinder, *ASP Conf. Ser.* 26, 549
 Stevenson, C. C. 1994, *MNRAS*, 267, 904
 Vogt, S. S. 1987, *PASP*, 99, 1214
 Wallerstein, G. 1972, *PASP*, 84, 656
 ———. 1979, *PASP*, 91, 772
 ———. 1983, *PASP*, 95, 422
 Wallerstein, G., & Elgar, S. 1992, *Science*, 256, 1531
 Wallerstein, G., Jacobsen, T. S., Cottrell, P. L., Clark, M., & Albrow, M. 1992, *MNRAS*, 259, 474
 Wesselink, A. J. 1946, *Bull. Astron. Inst. Netherlands*, 10, 91
 ———. 1969, *MNRAS*, 144, 297